

# Design and assessment of a small autonomous airborne observation platform

Frank Buysschaert<sup>1</sup>, Moaad Yacoubi<sup>1</sup>, Jérôme Sans<sup>1</sup>, Patrick Hendrick<sup>1</sup>  
Fryderyk Pomirski<sup>2</sup>, Mathieu Seiler<sup>2</sup>

<sup>1</sup>Université Libre de Bruxelles, Department of Applied Sciences, Aero-Thermo-Mechanics Laboratory  
50, F.D. Roosevelt Avenue, 1050 Brussels, Belgium

<sup>2</sup>Ecole des Mines d'Alès  
Avenue de Clavières, 30319 Alès, France  
email: frank.buysschaert@ulb.ac.be

## Abstract

**This paper gives an overview of the major disciplines involved in the design and construction of an autonomous ducted rotor UAV, developed to compete in the French Onera/DGA mini-drones contest. The concept as well as its prime components will be expounded, issues exposed and possible solutions addressed. First flight tests without stability system have shown the feasibility of the concept. Flight tests with an operational inertial reference unit is part of future work.**

## Keywords

**RUAV, MAV, UAS, duct, rotor, autonomous, IRU**

## I. INTRODUCTION

**I**N 2007, Onera (the French Office National d'Etudes et de Recherches Aéronautiques) launched a second inter-university competition for the design and the development of small airborne observation platforms or MAVs in cooperation with the French Ministry of Defense DGA (Délégation Générale de l'Armement). The goal of the competition, was finding new Unmanned Aerial System (UAS) technologies useful for military purposes, directly or indirectly, by funding several independent teams that battle for victory<sup>1</sup>, while developing diverse and sometimes exotic platforms using state-of-the-art components and/or construction techniques. The MAV must pass several milestones showing e.g. autonomous takeoff and landing, sufficient stability in perturbed atmospheres (gusts, steady wind) and so on. The Université Libre de Bruxelles (ULB, Belgium) was contacted by Ecole des Mines d'Alès (EMA, France), to help developing the UAS. It was then decided to use a Rotor Wing UAV (RUAV) configuration, based on a former design (Ema'tador, [1]) but smaller in size with only one rotor placed in a duct and with movable blades for control (Plate 1). The disciplines discussed in the subsequent sections are : *rotor and propulsion, aerodynamic design, structure and mass & balance, flight control system* and finally *data transmission and camera*. Each discipline will be described briefly. It is obvious that the operational ability of the RUAV not only depends on the successes made in several disciplines, but also by their capability to work as a whole system.

<sup>1</sup>and a financial reward, welcomed of course to compensate the additional expenses . . .

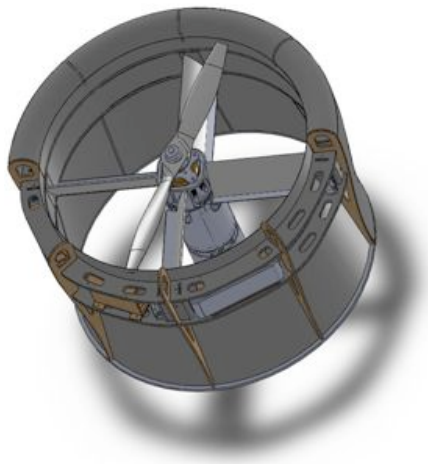


**FIG. 1.** CAD impression of the Dulbema RUAV. The lower duct cover has been removed to unveil the lightweight inner structure and a battery bay.



FIG. 2. The Dulbema main propulsion system components.

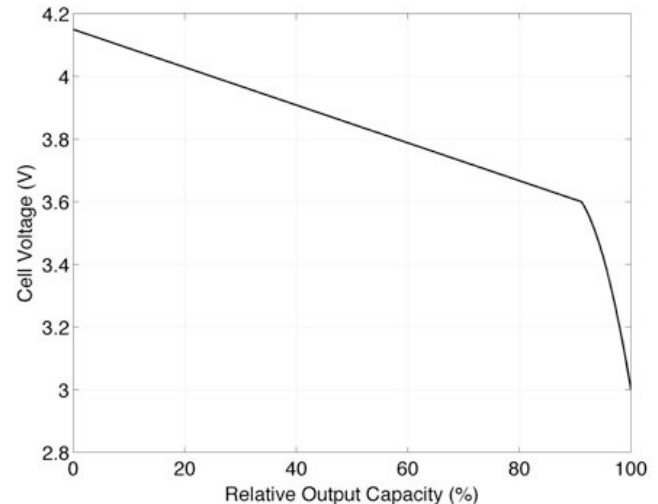


FIG. 3. LiPo battery cell voltage variation with output capacity (source ThunderPower Batteries Inc.).

## II. ROTOR AND PROPULSION SYSTEM

In a first stadium, the mission requirements must be specified. This includes a mission profile, minimum performance requirements, payload specifications - in this case a well performing camera - and the level of independence of the airborne platform with respect to the ground station. Here the MAV is demanded to navigate itself autonomously to targets of interest. Also, maximum dimensions (transportability) must be set. For the competition, the airborne platforms had to fit in a 70 cm side cube. All these parameters affect the mass of the RUAV and its power consumption, thus also define the rotor geometry and the propulsion system in general (i.e. engine, gearbox, batteries). Since an internal combustion engine makes lots of noise and heat, produces greasy and camera obscuring smoke and introduces sufficient vibrations to the structure, an electrical brushless motor, powered by high performance Lithium-Polymer batteries, turned out to be the best choice. The difficulty with such a combination is finding an energy efficient synergy between rotor, motor and batteries, while avoiding a gearbox which leads to a lower Empty Weight. From the experience gained with the Ema'tador project, one learnt that designing a rotor is a time consuming and complex business. As the prove of flight of the concept was a key requirement, the decision was made to lessen the initial complexity using an off-the-shelf model aircraft propeller. The selection was eased using a software program *Motocalc*. The program allows studying a combination of several engine and propeller configurations. The result of the study is a two bladed Menz 16/8 aircraft propeller driven by a Scorpion S4020-12 brushless motor. The energy comes from 4 ThunderPower LiPo batteries of 3850 mAh each. Plate 2 shows these components. During flight, the batteries are discharged, causing a gradual drop of the battery voltage (Plate 3). The maximum performance of the RUAV depends strongly on the maximum thrust of the rotor. This parameter in turn is a function of the maximum rotor speed, which is proportional to the maximum voltage applied to the engine. Since this voltage decreases with time while the battery is discharged, the performance envelope of the RUAV gets narrower, a problem becoming critical when appealing on the last 10% of the battery capacity. Therefore each flight should be preceded by a meticulous evaluation of the mission in order to maximize the chances of recovering the platform. Table I gives a summary of some technical features concerning the propulsion system. Future research will address the development of a new optimized rotor with the aid of CFD (*Fine/Turbo<sup>TM</sup>* of *Numecca Int.*) with special attention given to the interaction between duct and rotor.

## III. AERODYNAMIC DESIGN

A real challenge with this type of RUAV is dimensioning all components such that they perform well aerodynamically within the constraints set by, inter alia, the propulsion system<sup>2</sup> and mass & balance limits<sup>3</sup>. Besides, the RUAV must operate in hover and in translational flight with angles of attack ranging from 0° (climb), over 90° (horizontal flight) to 180° (descent), and this at various speeds and atmospheric conditions [2].

<sup>2</sup>By omitting for example the gearbox, the rotor must work at relatively high and variable angular velocities.

<sup>3</sup>It will be explained in Section IV that the control blades must be positioned as far as possible from the centre of gravity.

**TABLE I.** Propulsion system component parameters

<b>Brushless motor</b> <b>Scorpion S4020-12</b>	
$P_{max, Cont.}$ (W)	1500
$K_v$ (RPM/V)	542
$I_{max}$ (A)	85
$R_m$ ( $\Omega$ )	0.020
mass (kg)	0.304
<b>Lithium polymer batteries</b> <b>Thunder Power TP3850-3SXV</b>	
Capacity/unit (mAh)	3850
Cells/unit (-)	3
Unit voltage (V)	11.1
Mass/unit (kg)	0.384
Units installed aboard	4 (2x2)
<b>Propeller</b> <b>Menz 16/8</b>	
Diameter (m)	0.4064
Pitch (m/rev)	0.2032
Installed thrust (N)	43

A duct<sup>4</sup> can improve the thrust-to-power-ratio of the rotor [3]. The duct prevents the contraction of the rotor slipstream, an inevitable effect for free rotors, causing a drop in power consumption for a given total thrust  $\hat{T}$ . This positive effect is unfortunately weakened with increasing climb speed [4] (Plate 6). A ducted rotor becomes particularly interesting when used for stationary flight, an important phase in the mission specifications typical for RUAVs (observation, cargo release, ...). A major parameter influencing the power gain is the ratio of duct exit area ( $A_e$ ) to rotor area ( $A_R$ ) defined as  $a_d$  :

$$a_d = \frac{A_e}{A_R} \quad (1)$$

Plate 6 instigates the designer to choose a large  $a_d$ . Unfortunately, that would turn out to be a thoughtless choice. The theory behind this result only considers the induced power  $\hat{P}_i$  per unit of thrust  $\hat{T}$ . It does not account for interference losses (between rotor-duct and rotor-fuselage), nor for geometric related effects wherein the duct lip radius, chord length and profile thickness play an important role, nor for the external airflow conditions. Besides these shortcomings, one can neither deny the increase of weight by the installation of a duct, nor the harming effects of the important amount of profile drag present at the higher flight speeds, both demanding a higher thrust setting to remain in mechanical equilibrium. The duct profile drag coefficient without rotor installed  $C_D$  is shown on Plate 5, originating from first wind tunnel tests. Even for zero angle of attack ( $\alpha = 0^\circ$ ) for which the free stream velocity coincides with the duct vertical axis of symmetry, one obtains a rather high  $C_D$  and for some  $\alpha$  its value exceeds the lift coefficient  $C_L$  considerably (Plate 4). This effect has been confirmed by other studies such as [2]. Remark the typical positive effect a larger Reynolds number  $Re_\infty$  has on  $C_D$ , principally caused by flying faster. Similar results have been obtained for the duct lift coefficient  $C_L$  where a rise in  $Re_\infty$  increases  $C_{L,max}$  and smoothens the stall and post-stall behaviour. An important comment must be made concerning the definition of  $C_L$  and  $C_D$ . For ducted fans, one frequently uses the following

<sup>4</sup>The outside torus wherein the rotor is installed is called *duct*, while the centre part in which the rotor and motor are integrated is called *fuselage*.

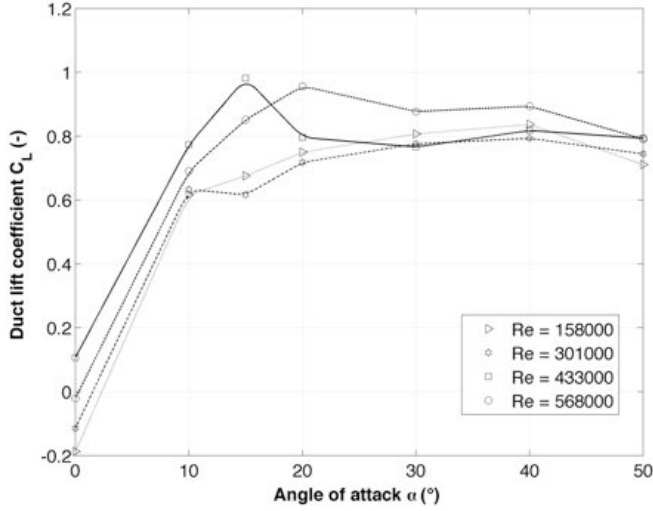


FIG. 4. Duct lift coefficient without rotor installed.

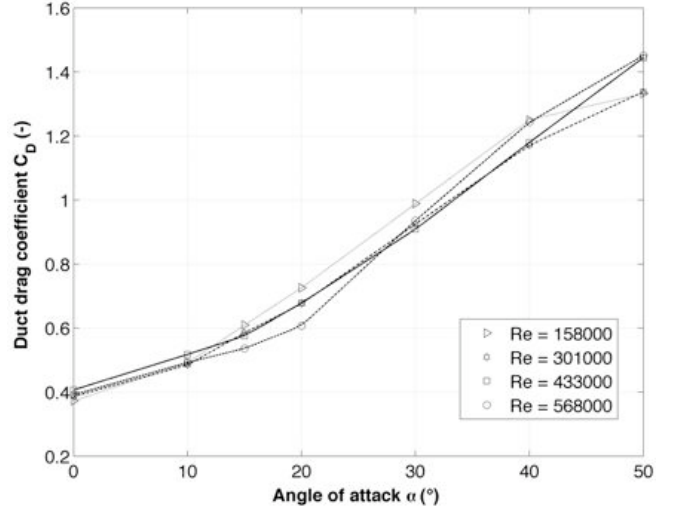


FIG. 5. Duct drag coefficient without rotor installed.

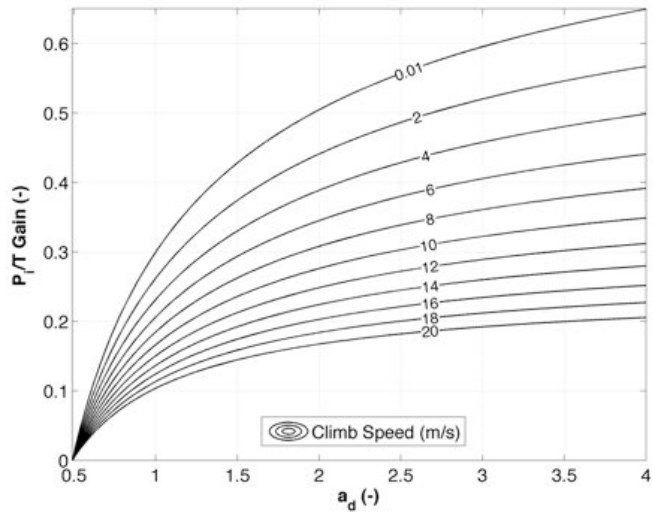


FIG. 6. Gain of rotor induced power  $\hat{P}_i$  per unit of thrust  $\hat{T}$  as a function of area ratio  $a_d$  and climb speed  $V_c$ .

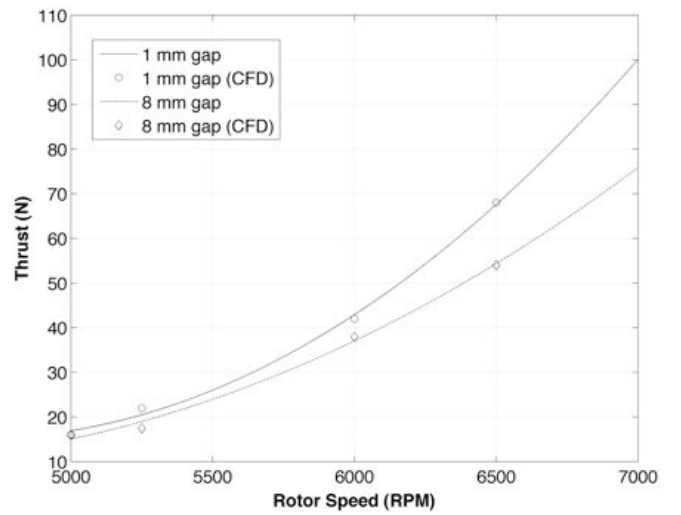


FIG. 7. Influence of the gap dimensions on the total thrust  $\hat{T}$  of a ducted rotor system.

convention [5][6] :

$$C_L = \frac{L}{qa_d A_R} \quad (2)$$

$$C_D = \frac{D}{qa_d A_R} \quad (3)$$

$$Re_\infty = \frac{\rho_\infty v_\infty D_e}{\mu_\infty} \quad (4)$$

Where  $q$  is the dynamic pressure of the free stream flow and  $D_e$  the diameter of the exit area  $A_e$ . Observe that a positive  $C_L$  is beneficial since it alleviates the rotor thrust requirement. Consequently,  $a_d$  should be chosen between 1 and 1.5. Wind tunnel tests complemented with CFD calculations seem here to be the best design, evaluation and validation tool. This is especially true for the integration of the rotor in the duct [7][8], where the gap between rotor tip and duct influences the total thrust of the RUAV. CFD calculations performed on this matter by one of the authors [9] confirmed the necessity of reducing the gap between rotor and duct as much as possible in order not to destroy thrust. Some of the results are reflected in Plate 7. Plate 8 and 9 unveil respectively a high axial and azimuthal velocity field near the gap explaining substantial interactions between the rotor tips and the duct wall. Some general aerodynamic characteristics are given in Table II. Another special asset of the RUAV concept is the obtention of flight

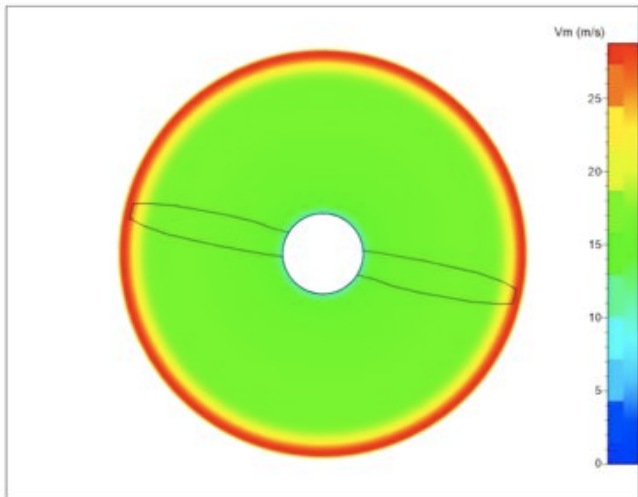


FIG. 8. Axial velocity field near the rotor plane, 5000 RPM.

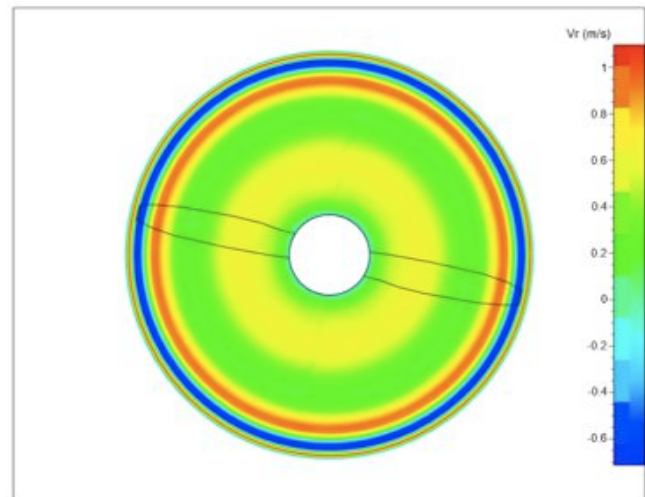


FIG. 9. Azimuthal velocity field near the rotor plane, 5000 RPM.

TABLE II. General aerodynamic characteristics

Duct diameter (m)	0.41
Duct chord (m)	0.30
Duct profile thickness-to-chord ratio (-)	0.15
Ratio of duct LE radius to rotor diameter (-)	0.11
$a_d$	1.1
Fuselage diameter (m)	0.08

controllability by putting blades in the downwash of the rotor. This requires a serious aerodynamics and performance exercise because the rotorcraft must remain controllable in all flight conditions where the downwash is a function of the thrust setting, the atmospheric conditions and the speed component. Also, for a given weight, altitude and speed vector, the aerodynamic/inertial forces and moments must be known and dealt with by the rotor and control blades to assure a stable flight condition. Plate 10 elucidates the architecture of the flight control system. One can distinguish two rows of blades. The upper blade row serves as anti-torque mechanism, used to compensate the torque put by the electric motor on the structure, but also vouches for sufficient yaw control. The anti-torque blades have flaps on the trailing edge (Plate 11), which is mandatory to gain acceptable levels of controllability. To ensure adequate structural stiffness, the blades cannot not be made all movable and therefore it becomes important to mount these stators on the fuselage under a correct angle of attack with respect to the downwash of the rotor. Indeed, the downwash leaves the rotor with a corkscrew motion and thus has an azimuthal speed component, as shown on Plate 9. This in combination with the vertical component of the downwash results into a certain incidence angle  $\gamma$  measured from the vertical axis of symmetry of the duct. CFD calculations in a modified version of *Fine/Turbo<sup>TM</sup>* allowed determining this incidence angle  $\gamma$  (Plate 12) and the flow behaviour around the anti-torque blades in the rotor downwash (Plate 13). The magnitude of  $\gamma$  increases with the radius  $r$ , reaching a maximum close to the rotor tip radius  $R$ . Also,  $\gamma$  increases with the angular speed of the rotor. This means that at the highest thrust settings the outer part of the anti-torque blade is prone to get stalled before the other sections do (example on Plate 13). This is a dangerous situation as the outer part generates most of the anti-torque, because it has the largest moment arm around the centre of gravity while being placed in the area with the highest downwash velocity (Plate 8). Currently, the anti-torque blades are untwisted to reduce development time and costs, though it is mandatory that future designs of the anti-torque blades will incorporate (non-)linear twist and have variable angles of incidence instead of using trailing edge flaps to improve the performance and control margin of the RUAV. Clearly, wind tunnel tests will be necessary to verify the effectiveness of the anti-torque system while flight testing will be the ultimate judge. The lower row of symmetrical blades on Plate 11 enables pitch and roll control. Since

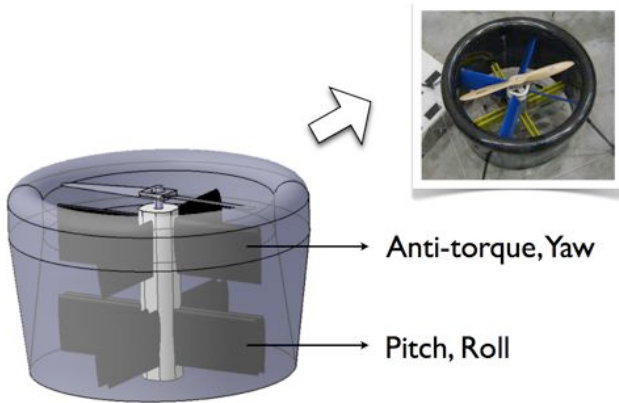


FIG. 10. Two blade rows must produce sufficient anti-torque, pitch, roll and yaw control.

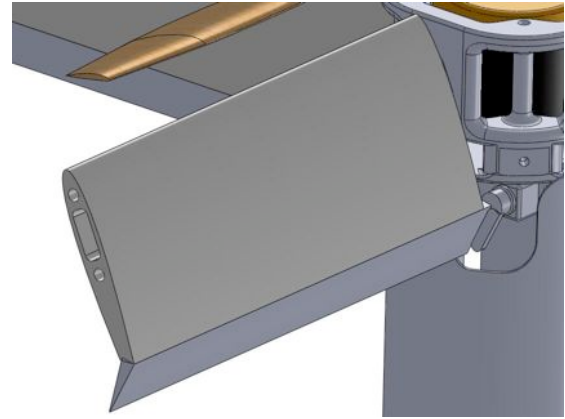


FIG. 11. The anti-torque blades are equipped with a trailing edge flap.

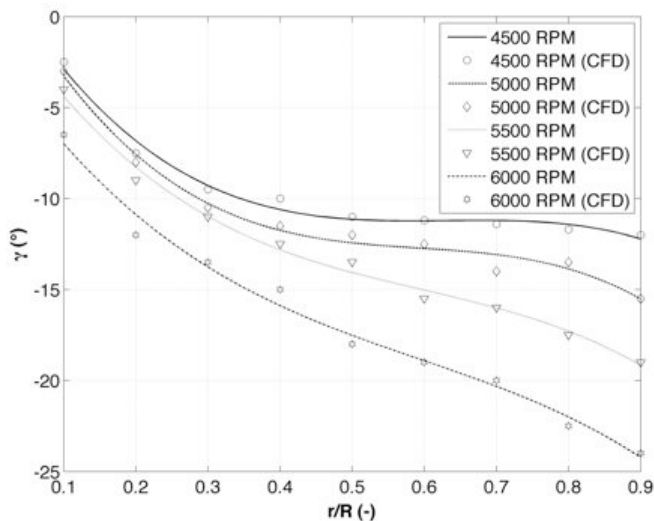


FIG. 12. Downwash angle of incidence  $\gamma$  as a function of radial position  $r/R$  and rotor speed.

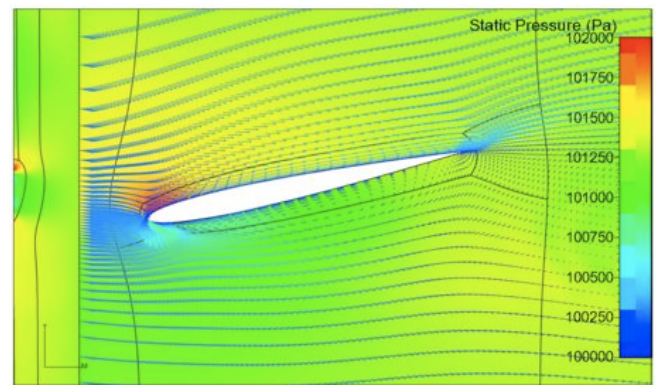


FIG. 13. The outer part of the untwisted anti-torque blade gets stalled earlier than the inner part ( $r/R=0.9$ , 5000 RPM,  $\dot{m}=2.6$  kg/s).

the exerted forces on the lower part of the airframe are less important, it was possible to give these blades a variable angle of incidence instead of using trailing edge flaps. Several blade profiles were examined with *Xfoil*. The blade chord dimensions for both blade rows depend strongly on the required rotor power and aerodynamic characteristics of the duct, but they are also particularly sensitive to the position of the centre of gravity. Remark that for the lower row, a biplane configuration has been selected in order to avoid a longer fuselage, which would result in a higher Empty Weight and more drag.

Before ending this section, it is important to examine one more flight condition that is sometimes forgotten. “*What comes up, must come down*”, many of us quote. Preferably, the descent is stable and controlled. For rotorcraft, the descent is a wolf in sheep’s clothing. Many rotorcraft crashed in the early days during this flight phase (and sometimes they still do) because they arrived in a then badly understood but now commonly called *Vortex Ring State*, where the rotor turns in its own wake, causing the descent to become highly unstable and mostly followed by significant descent rates. The phenomenon occurs when descending at a rate  $V_d$  of the order of magnitude of the induced rotor speed  $v_i$ . For a ducted rotor, this becomes the velocity at the exit of the duct  $\hat{v}_i$ . With  $V_d$  larger than twice  $\hat{v}_i$ , the flow through the duct gets reversed. For increasing descent rates starting from hover, the streamlines bend upwards somewhat downstream the duct exit, afterwards continuing their way up with the free stream flow. Plate 14(a), representing the airflow at  $V_d$  equal to about a quarter of  $\hat{v}_i$ , shows however that some of the streamlines (represented by red lines) are diverted back

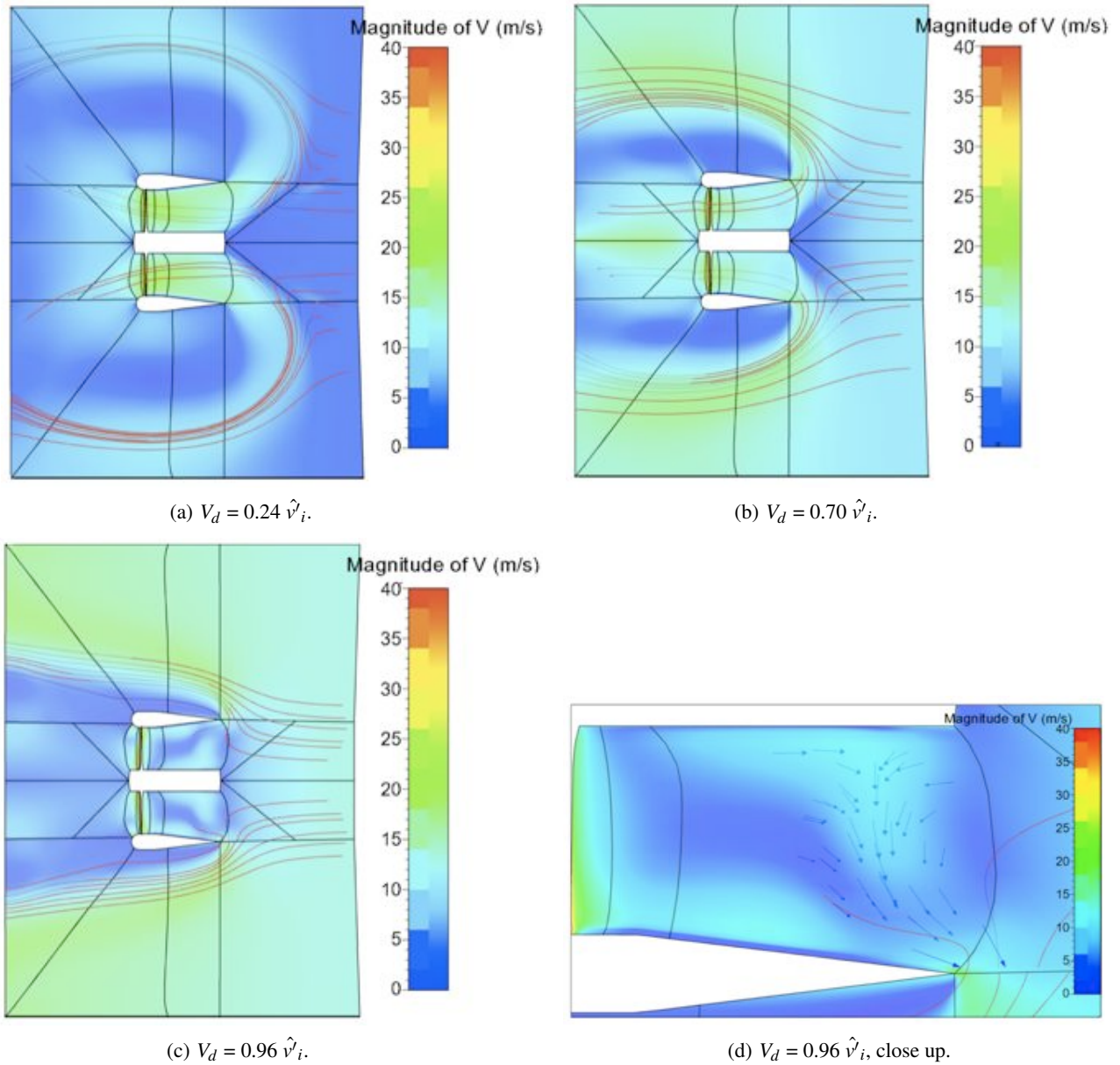


FIG. 14. Influence of the descent speed  $V_d$  on the flow field.

into the duct<sup>5</sup>. When  $V_d$  reaches three quarters of  $\hat{v}_i$  (shown on Plate 14(b)), the “inflexion” point downstream the rotor approaches the exit of the duct causing the upward flow to block the exit area even more. The downwash velocity is the lowest near the centre of the duct and logically this zone gets affected first. When  $V_d$  tends towards  $\hat{v}_i$ , there is almost no room left to expel the air from the duct, as shown on Plate 14(c). Now, the flow can only leave the duct via the area adjacent to its walls. Inside the duct, a strong recirculation zone appears (Plate 14(d)). This phenomenon effectively destroys the pitch and roll authority of the RUAV as the velocity field over the lower row blade stack gets seriously perturbed. Results for larger descent rates could unfortunately not be obtained due to non converging calculations. Nevertheless an important conclusion could be drawn : a ducted RUAV is also liable to unstable phenomena during descent, causing loss of control. The descent rate should not approach the induced speed ruling at the exit of the duct.

#### IV. STRUCTURE AND MASS & BALANCE

Needless to say that the use of high quality composite materials is mandatory when pursuing a stiff and lightweight structure. High stiffness allows the distance between the rotor and duct to be minimized, an important requirement

<sup>5</sup>This phenomenon is also believed to be caused partially by a too small meshing volume in which the RUAV model was created.

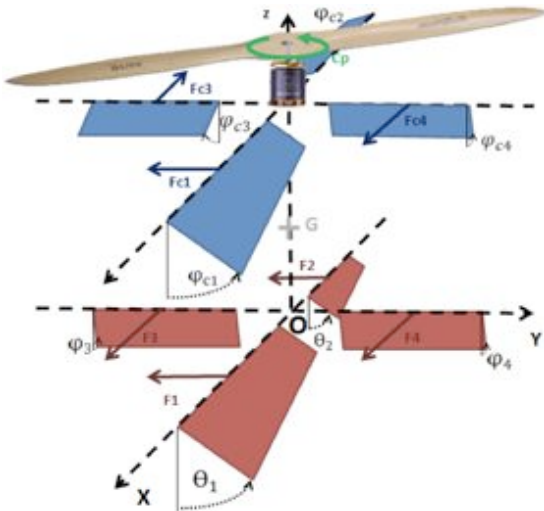


**FIG. 15.** Sufficient distance between the center of gravity (G) and the application points of the control blade forces must be strived for.

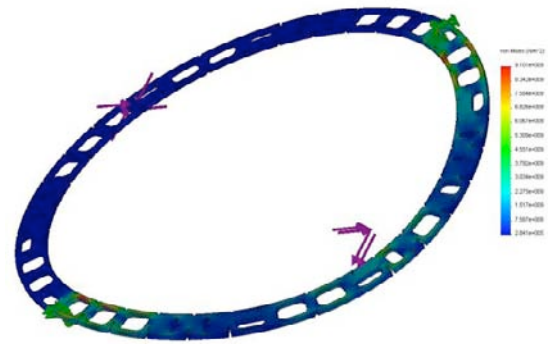


**FIG. 16.** The balsa ribs are fixed on PMMA rings (first prototype). Each ring is a critical part : it keeps the rather heavy batteries in place and guarantees the circular shape of the duct.

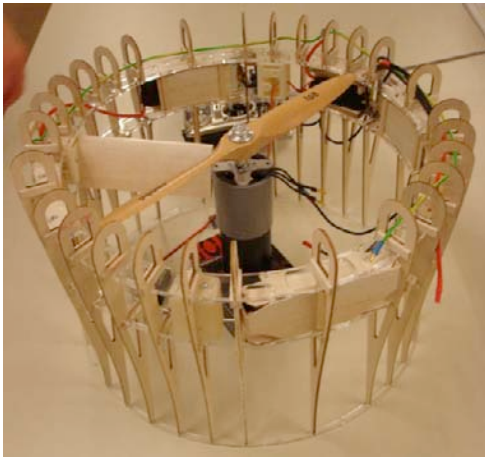


**FIG. 17.** Extensive use of balsa wood helps reducing the weight significantly.

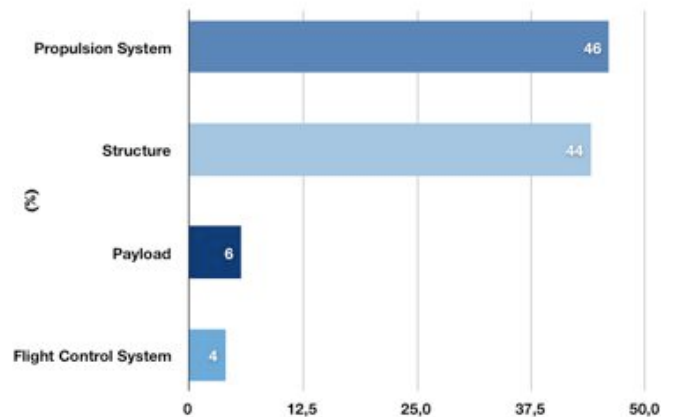


**FIG. 18.** Main components mass distribution, with a total mass of approximately 3.5 kg.

which has elaborately been examined in the aerodynamics section. This minimization is not without risks as it increases the possibility of an impact of the rotor with the duct walls behind which the batteries are installed. Another important parameter is the position of the center of gravity relative to the rotor and the duct suspension planes since it influences the inertial forces exerted on the platform, the required aerodynamic forces to gain controlled flight and thus the necessary structural strength and associated weight [10]. The higher the center of gravity is positioned, the more control authority will be obtained, but one should avoid doing so by lengthening the duct and fuselage since this increases the weight of the platform, which is an unwanted effect for reasons explained before (Plate 15). The best way to comply with this condition is by installing the heaviest parts such as the batteries in the upper part of the platform. To optimize the structure, thorough FEM calculations in *Solidworks* will be necessary (Plate 16), while modal analysis will allow the rotor to work at frequencies sufficiently remote from the critical frequencies. Besides the use of carbon composites for the duct and fuselage skin, balsa wood was selected for the ribs of the control surfaces and the duct (Plate 17), while glass fiber reinforced plastics assure adequate strength for the installed landing gear. Plate 18 gives an overview of the total mass distribution over the main components.



**FIG. 19.** MTi-G IRU (orange box) and circular print plates upon which CPUs will be soldered. The circular shape of the print plates increases the useful area available for the electronic components and facilitates the installation and fixation when placed in the cylindrical fuselage.

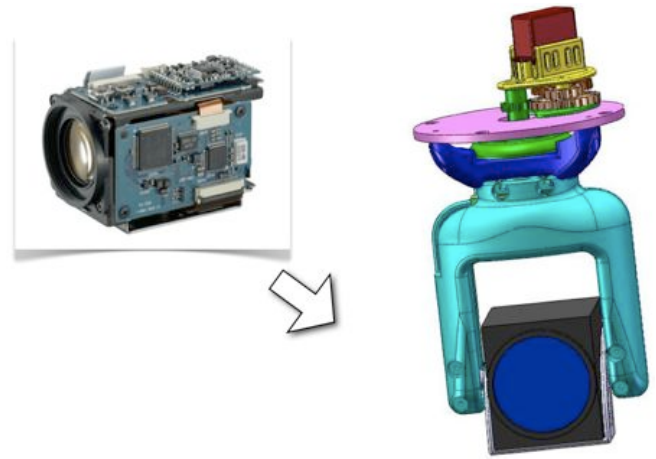


**FIG. 20.** A powerful lightweight camera installed on a flexible platform makes a perfect combination.

## V. FLIGHT CONTROL SYSTEM

Key elements of the flight control system are the inertial reference unit (IRU) and the control-electronics. These components must determine the position of the RUAV with respect to the earth coordinate system, steer the RUAV towards the selected waypoints and targets and keep a balanced flight at all times (including takeoff and landing). This is done with the aid of a GPS receiver, accelerometers, an electronic compass and gyroscopes, all integrated in the IRU, installed in the fuselage of the RUAV. The IRU-signals enter an in-house made controller wherein consequently software determines the propeller angular velocity and the required angle settings of the control blades, brought in position via servos installed in the fuselage, and eventually used to control the position of the aircraft (Plate 19). Table III summarizes technical information of the IRU unit. The IRU unit should normally be installed in the center of gravity, which requires a detailed CAD analysis. In order to electrically uncouple the flight control system from the propulsion system, a separate battery pack is foreseen in the fuselage.

## VI. DATA TRANSMISSION AND CAMERA

Besides the requirement that the RUAV must be able to fly its mission autonomously at all times, a live video stream must be guaranteed to enable the operator to inspect the (pre)determined targets from a ground station. Meanwhile, a flight command data link must assure the ability to instantly modify or cancel parts of the flight plan. The live video stream undergoes special software treatment of IMINT Image Intelligence AB (SE) to stabilize the image. The software allows the operator to inspect the target easily cancelling out all vibrations and unwanted image shifting, even when a high optical zoom is selected. This increases the efficiency of the platform and probably its operational range (more flying time, less detecting time). The camera will be installed on the lower extremity of the fuselage and is fed by the flight control system battery pack. A sophisticated mechanical system allows the camera to pitch horizontally and vertically (Plate 20). Table IV gives an overview of typical characteristics of the camera.

**TABLE III.** MTi-G Inertial Reference Unit

<b>GPS</b>	
Receiver type	16 channels, L1 frequency, C/A code
GPS Update Rate (Position / Velocity)	4Hz / 120Hz
Accuracy Position SPS	2.50 m
Maximum altitude	18 km
Maximum velocity	515 m/s

<b>Interfacing</b>	
Digital	RS-232
Operating voltage	4.5-30 V
Power consumption	540 mW

<b>General data</b>	
Dimensions (WxDxH)	58x58x33 mm
Mass	68 g
Ambient temperature operating range	-20 ... 55°C

**TABLE IV.** Camera specifications

<b>SONY FCB-IX11AP Camera</b>	
Image sensor	1/4 type Exview HAD CCD
Effective pixels	440 000
Lens optical zoom	10x
Lens digital zoom	4 x
Minimum illumination	1.5 lux
Video output	PAL
Operating temperature	0 ... 50°C
Power consumption	1.6 ... 2.1 W
Supply voltage range	6 ... DC 12V
Mass	95 g
Dimensions (WxHxD)	39.3x44.8x65 mm

## VII. CONCLUSIONS AND PERSPECTIVES

Until now, only flight tests at slow horizontal speeds and hover were performed without the flight control system incorporating the IRU (Plate 21). Piloting the MAV manually remains a demanding job for an inexperienced pilot because of the severe coupling between the pitch, roll and yaw axes. This clearly proves that a sophisticated flight control system will be indispensable. Wind tunnel tests evaluating a broad flight envelope are performed at the time of writing, which will allow to examine and expand the flight envelope of the MAV considerably and in a safe way, directly or indirectly via CFD. As a consequence of the chosen RUAV concept, better hover performance can be achieved thanks to the installation of a duct, however it was shown that then the aerodynamic and structural design are heavily interrelated. CFD calculations allowed the evaluation of the anti-torque blade incidence angle settings and exposed a dangerous descent condition which must be avoided in order to maintain flight controllability. Also, special attention was given to the fact that the position of the center of gravity significantly affects the aerodynamic and structural design parameters and should therefore be closely monitored with the aid of a CAD program. Although not yet apt to fly autonomously, the Dulbema is on the verge of exploring its potential.



**FIG. 21.** Hover flight without the installation of the complex and expensive IRU-equipped flight control system.

#### REFERENCES

- [1] Hendrick, P. and Depouhon, A., *Optimal control strategies for a ducted RUAV*, RTO AVT, Firenze, Italy, 2007.
- [2] Parlett, L.P., *Aerodynamic characteristics of a small-scale shrouded propeller at angles of attack from  $0^\circ$  to  $90^\circ$* , NACA TN 3547, Langley Aeronautical Laboratory, Langley Field, VA, USA, 1955.
- [3] Leishman, J.G., *Principles of helicopter aerodynamics*, Cambridge University Press, Cambridge, UK, 2002.
- [4] Newman, S., *The foundations of helicopter flight*, Butterworth Heineman, Oxford, UK, 1994.
- [5] Kriebel, A.R. and Mendenhall, M.R., *Predicted and measured performance of two full-scale ducted propellers*, NASA Contractor Report CR-578, Washington DC, USA, 1968.
- [6] Mendenhall, M.R. and Spangler, S.B., *Theoretical study of ducted fan performance*, NASA Contractor Report CR-1494, Washington DC, USA, 1970.
- [7] Pereira, J. and Chopra, I., *Effect of shroud design variables on hover performance of a shrouded-rotor for micro air vehicle applications*, American Helicopter Society Paper AHS 2005, Alfred Gessow Rotorcraft Center, Department of Aerospace Engineering, University of Maryland, College Park, MD, 2005.
- [8] Ahn, J., *Parametric design of a ducted fan system in forward flight and static conditions*, American Helicopter Society Paper AHS 2005, Dept. of Aerospace Engineering, Sejong University, Seoul, Korea, 2005.
- [9] Sans, J., *Conception et réalisation d'un mini-drone à décollage vertical*, Master Thesis, Université Libre de Bruxelles, Brussels, Belgium, 2009.
- [10] Josephs, H. and Huston, R., *Dynamics of mechanical systems*, CRC Press, Florida, USA, 2002.